



Contents lists available at ScienceDirect

## Journal of the Mechanics and Physics of Solids

journal homepage: [www.elsevier.com/locate/jmps](http://www.elsevier.com/locate/jmps)

# The collusion of flexoelectricity and Hopf bifurcation in the hearing mechanism

Qian Deng<sup>a</sup>, Fatemeh Ahmadpoor<sup>b</sup>, William E. Brownell<sup>c</sup>, Pradeep Sharma<sup>b,d,\*</sup><sup>a</sup> State Key Laboratory for Strength and Vibration of Mechanical Structures, School of Aerospace, Xi'an Jiaotong University, Xi'an, Shaanxi, China<sup>b</sup> Department of Mechanical Engineering, University of Houston, Houston, TX, USA<sup>c</sup> Department of Otolaryngology-H & NS, Baylor College of Medicine, Houston, TX, USA<sup>d</sup> Department of Physics, University of Houston, TX, USA

## ARTICLE INFO

## Article history:

Received 23 April 2019

Revised 27 May 2019

Accepted 30 May 2019

Available online 11 June 2019

## ABSTRACT

How do the weak sound waves get amplified in a cochlea? This deceptively simple question has attracted a fair amount of attention and several creative mechanisms have been proposed that purport to understand how the inner ear's hair cells actively collude to achieve the requisite sensitivity, frequency selectivity, range and nonlinear amplification. Some of the proposed mechanisms target the nature of the mechanoelectric transduction mechanism while others adopt a more dynamical systems approach and focus on the fact that stereocilia of the hair cells operate on the verge of an instability phenomenon—the so-called Hopf bifurcation. In this work, we propose a physics-based model to understand how flexoelectricity, a universal electromechanical coupling that exists in all dielectric substances, facilitates the mechanics of the active motion of hair bundles. A key feature of our model is that we eschew a “black-box” approach, and all parameters are well-defined physical quantities such as membrane bending modulus, geometrical characteristics and others. Furthermore, the model is derived from the well-accepted principles of mechanics and soft matter physics. While the role of flexoelectricity in the hearing mechanism has been noted before, we show for the first time that flexoelectricity is an *essential* ingredient in inducing the Hopf bifurcation state considered responsible for several highly nonlinear and peculiar features of the hearing mechanism. We find that the biomembranes' bending modulus and the intracellular charge concentration (which for instance could represent  $K^+$  or  $Ca^{2+}$ ) are the two key control parameters that significantly impact the stability of the system and hence the hearing mechanism. Our work highlights the importance of flexoelectricity, confirms earlier assertions that the cochlea amplifies the acoustic stimuli through its exceptional electromechanical energy conversion property, and provides insights into how physical properties such as biomembranes' bending modulus impact the performance of the hearing system.

© 2019 Elsevier Ltd. All rights reserved.

## 1. Introduction

The hearing system is a soft machine *extraordinaire* that collects and processes airborne sound waves in a manner that defies any man-made audio-processing device. Human ears, for instance, can distinguish one-thirtieth of the frequency dif-

\* Corresponding author at: Mechanical Engineering, University of Houston, 4800 Calhoun Road, Houston, TX 77204, United States.  
E-mail addresses: [psharma@central.uh.edu](mailto:psharma@central.uh.edu), [psharma@uh.edu](mailto:psharma@uh.edu) (P. Sharma).

ference between two successive piano keys which are just a semi-tone apart, have an auditory range that spans three orders of magnitude (20 Hz–20 kHz), and can handle a million-fold variation in amplitude (Hudspeth, 2014; Martin and Hudspeth, 2001). Remarkably, the fluid filled sensor, cochlea, is so sensitive that even a signal that vibrates the eardrum by merely a picometer can be detected (Dalhoff et al., 2007; Hudspeth, 2014; Maoileidigh and Hudspeth, 2013). The energy of incoming sound waves dissipates quickly in the viscous liquid that fills a cochlea but there is strong evidence that the ear actively supplies energy to compensate for this dissipation. Since the pioneering work of Gold (1948) in the late forties, it is now well-accepted cf. (Camalet et al., 2000; Choe et al., 1998; Hudspeth, 2005; Hudspeth et al., 2010; Maoileidigh and Hudspeth, 2013) that the ear is not a passive sensor but actively aids in the process of audition. As eloquently articulated in the following reviews and expositions (Hudspeth et al., 2010; Nadrowski et al., 2004), this active trait of the ear is encapsulated by the following three attributes: *amplification*, *compressive nonlinearity* and *tuning*. The *amplification* denotes the ability of the ear to amplify a weak sound it collects. This feature effectively decreases the threshold for the sound detection of the ear. With an active process, weak input acoustic signals can be amplified by several hundred times in amplitude (Martin and Hudspeth, 1999; 2001). The *compressive nonlinearity* exhibited by the human ear allows exceptional sensitivity to even the faintest sound while simultaneously possessing the capability of enduring the roar of jet engines. Notably, although the amplitude of the weakest and strongest sound waves that can be handled by the ear spans a million fold (from picometres to microns), the actual response within the cochlea is compressed into only a hundred fold (several nanometers to hundreds of nanometers) in range (Eguiluz et al., 2000; Hudspeth et al., 2010; Kern and Stoop, 2003; Martin and Hudspeth, 2001). In other words, if the input signal is weak, the cochlea amplifies it “sufficiently” however if it is very strong, as a protection mechanism, the amplitude of vibration are attenuated by the active process. Finally, the *tuning* feature endows the mammalian ears with a rather sharp frequency selectivity (Spiegel and Waltson, 1984).

The active processes and the features of the hearing mechanisms mentioned in the preceding paragraph are intimately related to the hair cells located in the cochlea. While the mammalian and non-mammalian hearing mechanisms differ in several respects, they share many common features and exhibit several similar characteristics outlined in the preceding paragraphs. Specifically, the hair bundle’s motility is believed to play an important role in the active process of the cochlea, for both mammals with outer hair cells (Chan and Hudspeth, 2005; Kennedy et al., 2005; Maoileidigh and Juicher, 2010) and non-mammals in which they are absent (Choe et al., 1998; Fettiplace and Kim, 2014; Hudspeth, 1997; Tinevez et al., 2007). Our work focusses primarily on hair bundle motility although it is likely to have ramifications to understand somatic motility also. In the interest of brevity, we avoid further discussion of *somatic* motility and simply refer the reader to the literature (and references therein) cited in this paragraph for further information.

So far, in our opinion, there are two key open questions pertaining to hair bundle motility:

1. How does the hair-bundle motility boost the active process in cochlea?
2. How does the hair-bundle achieve its electromotility?<sup>1</sup>

The most widely accepted explanation that purports to address the first question is based on the unstable nonlinear oscillation of the hair bundles. The schematic in Fig. 1(a)–(d) presents the main ideas. Although the hair bundle motility is critical to the hearing of both mammals and non-mammals, in this paragraph, we will primarily focus on the non-mammalian hearing mechanism. Fig. 1(a) shows the cross-section of the receptor organ in the hearing organ of a generic non-mammalian vertebrate. The organ contains hair cells located on top of the basement membrane (BM). As can be seen in the figure, the tip of each hair bundle penetrates into an accessory noncellular structure. This acellular structure is located right above the hair cells. As the acoustic wave propagates in the BM, it causes the vibration of the hair cells and the hair bundles. Normally, each hair bundle consists of dozens to hundreds of actin based microvilli called stereocilia. The stereocilia within the same hair bundle have differing lengths. They are aligned in an orderly way to form a wedge shape. The schematic drawing for a hair bundle is shown in Fig. 1(b). For simplicity, only three stereocilia of the bundle are shown. Each stereocilia is connected to its neighbor by a fine and elastic molecular strand called the tip link. It is believed that, located on each stereocilia and around the connection with the tip link, are several mechano-sensitive ion channels (Camalet et al., 2000; Hudspeth, 1989; 2005). When the hair bundle is deflected, the increase of tip-link tension causes the opening of the ions channel gates and allows the influx of ions (both  $K^+$  and  $Ca^{2+}$ ). The actual relationship between the tip link force and the channel gate is complex. Power and coworkers proposed a biophysical model to analyze how the force that arise in tip links influence the channel of the stereocilia (Power et al., 2014; 2012). Since the tip link force depends on the deflection of a stereocilia, the probability of the channel’s open-state is thought to be a nonlinear function of the stereocilia deflection. Fig. 1(c) shows that the vibration of a stereocilia is actively coupled with the charge flow through its channel gates (Choe et al., 1998; Maoileidigh and Hudspeth, 2013). This active motion of the stereocilia is able to amplify a vibration with small amplitude into another with much larger amplitude. The nonlinear electromechanical behavior of the stereocilia

<sup>1</sup> At least for high frequency oscillations. The hair bundle’s motility can be both slow and fast adapted (Hudspeth, 2014). The slow adaption is believed to be related to the molecular motor, Myo1c, a member of the myosin family (Batters et al., 2004). Experiments indicate that small clusters of Myo1c molecules are essential to keep tip-links under tension, which cause the reopening of the ions channel gates (Grati and Kachar, 2011). The entry of cations provokes the slipping down of the upper insertional plaque of the tip-link attached to the longer stereocilia and causes the closure of the ions channel. Then the Myo1c reopens the channel by increasing the tension in the tip-links which causes the further deflection of the hair bundle in the direction of the stimulation. In this way, the energy is fed into the oscillation of the hair bundle. However, the fast adaption mechanism is still poorly understood (Hudspeth, 2014).

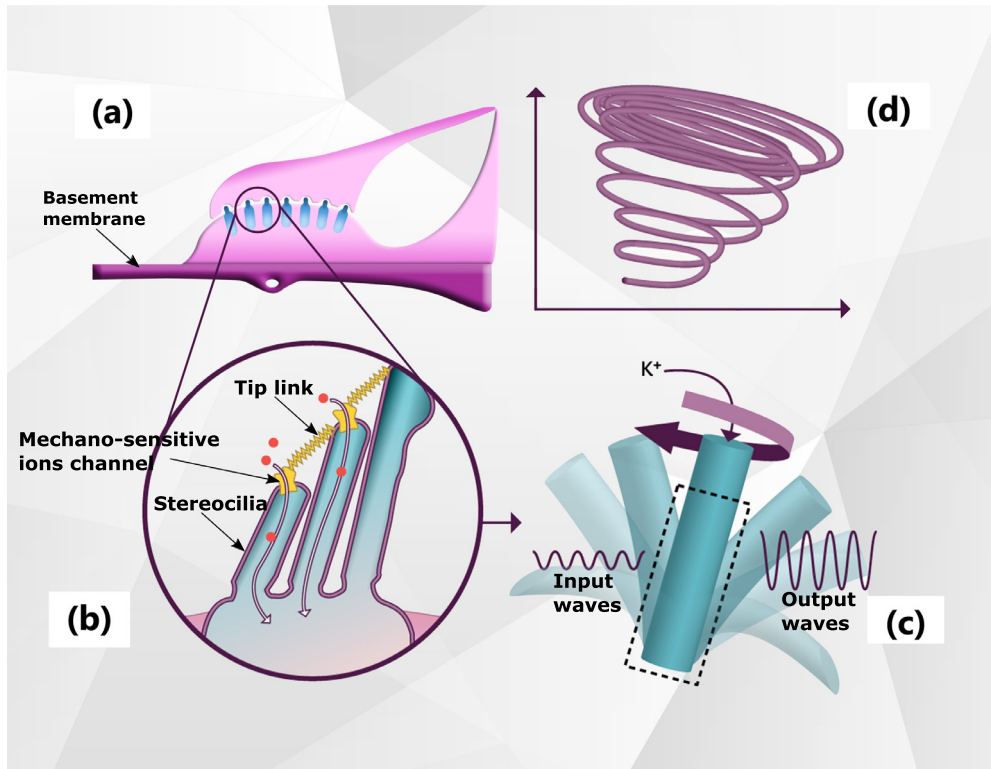


**Fig. 1.** The key ideas pertaining to the active process and its importance to the amplification function of the hearing system are described by Fig. 1(a)–(d). Fig. 1 (a) shows a cross-section of the receptor organ in the hearing organ of a generic non-mammalian vertebrate. Located on top of the basement membrane, there are hair cells whose hair bundles penetrate into the upper tectorial membrane. The acoustic wave propagating in the basilar membrane causes the vibration of the hair cells and the hair bundles. The hair bundle itself consists of “hair-like” objects called stereocilia. As shown in Fig. 1(b), each stereocilia is connected to its tallest neighbor by a fine molecular strand called tip link. It is believed that, located on each hair bundle and around the connection with the tip link, are several mechano-sensitive ion channels. When the hair bundle is deflected, the increase in tip-link tension causes the opening of the ion channel gates which allows the influx of ions (both  $K^+$  and  $Ca^{2+}$ ). The charge flow triggers the active motion of the hair bundle through a (somewhat debated) electromechanical coupling mechanism. As shown in Fig. 1(c), since the charge flow changes the voltage of the hair bundle, it affects the shape and consequently the motion of each stereocilia. Evidently, nature has evolved to tune parameters like ion concentration, the membrane’s bending stiffness and even the length and spring constant of the tip links, in subtle ways, so that the system runs on the verge of the so-called Hopf-bifurcation (Fig. 2(d)). Being on the verge of instability is speculated to be the key mechanism that allows the amplification of weak sounds in a rather specific way and several other critical and idiosyncratic features.

is thought to be the reason for the active motion and the amplification. As the charge flow changes the transmembrane electric field, due to the electromechanical coupling, the shape and consequently the motion of the stereocilia also changes accordingly. Nature appears to have well-tuned the parameters of the whole system, such as: the ion concentration, the membranes’s bending stiffness and even the length and spring constant of the tip links, so that it runs on the verge of the so-called Hopf-bifurcation. Fig. 1(d) shows the trajectory for the motion of a stereocilia in the phase space. As shown in the figure, if a perturbation slightly displaces the system away from its stationary point, then the system starts oscillating due to the loss of stability of the system. With the passage of time, the radius of the oscillation keeps increasing until the system eventually enters a limit cycle with a relatively larger radius.

The second question is related to the origin of the electromechanical coupling in stereocilia. Although the electromechanical coupling plays a critical role in the whole process, currently, the precise mechanism for the electromechanical coupling in stereocilia is still under debate. The electromechanical coupling is reminiscent of “piezoelectricity” observed in certain hard crystals, but there is no basis to believe that stereocilia are “piezoelectric” as they lack the atomistic structure to act that way. The myosin-based mechanism mentioned above is thought to be effective for low frequency (less than  $1\text{kHz}$ ) hair bundle motions (Hudspeth, 2014). For high frequency motions, a mechanism based on the cation’s concentration-sensitive channel is proposed (Hudspeth, 2005; Maoileidigh and Hudspeth, 2013). It has been argued that each channel is anchored to the stereocilia cytoskeleton by an adaptation spring whose stiffness decrease with the increase of the  $Ca^{2+}$  concentration. As the channel is open,  $Ca^{2+}$  ions flow in and release the tension in the adaptation spring. Then the reduction of the tension in adaptation spring causes the closure of the channel. Maoileidigh and Hudspeth have shown that, during these open-close cycles, energy is fed into the system in terms of the  $Ca^{2+}$  current flow. This process is much faster than the myosin-based process and could account for fast adaption (Maoileidigh and Hudspeth, 2013). Lumpkin and Hudspeth believe that the free  $Ca^{2+}$  concentration in a stereocilia is critical to its adaption process and have developed a model for stereociliary  $Ca^{2+}$  homeostasis (Lumpkin and Hudspeth, 1998). We remark here that *flexoelectricity*, like electrostriction, is a

universal electromechanical coupling mechanism that is present in *all* dielectrics including of course biological membranes (Ahmadpoor and Sharma, 2015). There are strong indications in the work of Brownell, his colleagues and others that flexoelectricity is a key element of the hair bundle's electromotility (Breneman et al., 2009; Brownell et al., 2001; Krichen and Sharma, 2016; M. Raphael et al., 2000).

While substantial research has been performed by several groups elucidating the myriad aspects of the hearing mechanism, we highlight a few that the current work is based on. Hudspeth's group was probably the first to link the active process in cochlea with the dynamical instability–Hopf-bifurcation (Chan and Hudspeth, 2005; Choe et al., 1998; Hudspeth, 2005; Martin and Hudspeth, 1999; 2001). In their model, the motility of hair bundles plays a critical role to link the charge flow to the active motion of the outer hair cells and the Hopf-bifurcation, the characteristic of the nonlinear system they construct plays an essential role in the amplification process. Brownell and his collaborators have advocated the viewpoint that membrane flexoelectricity is the source for the electromechanical coupling in hair bundles (Breneman et al., 2009; Brownell et al., 2001; M. Raphael et al., 2000). Using a theoretical model, they have shown that flexoelectricity is a possible source for the hair bundle's fast adaption (Breneman et al., 2009). The flexoelectric effect, first observed in liquid crystals (Meyer, 1969), is a universal two-way electromechanical coupling phenomenon in dielectric materials. Mathematically, flexoelectricity links the polarization to the gradient of deformation of materials via the material property parametrized by the so-called flexoelectric coefficient. Petrov (Petrov, 2001; 2006; Petrov and Sokolov, 1986) has argued that flexoelectricity of the nanometer thick biomembranes is the basic mechanoelectric effect for living matter. Within a lipid bilayer membrane, lipids are organized to form a liquid crystal membrane. This membrane exhibits a strong flexoelectric response due to its small thickness ( $\sim 1$  nm) and low bending stiffness ( $\sim 10^{-19}$ J). In a lipid bilayer membrane, the polarization caused by the direct flexoelectric effect is proportional to its mean curvature (Petrov, 2001; 2006; Petrov and Sokolov, 1986). A phenomenological expression for this relationship is given by:

$$p_s = \mu H, \quad (1.1)$$

where  $p_s$  (in C/m) is the electric polarization per unit area,  $H$  (in 1/m) denotes the membrane's mean curvature (defined as the sum of the membrane's two principal curvatures) and  $\mu$  (in C) is the area flexoelectric coefficient. Note that  $p_s$  relates to the polarization volume density  $P$  by Deng et al. (2014b) and Ahmadpoor et al. (2013)

$$p_s = Ph. \quad (1.2)$$

where  $h$  is the thickness of the membrane. The direction of  $p_s$  is assumed to remain normal to the middle plane during the deformation. Since the coupling between  $p_s$  and  $H$  is two-way, a change in  $p_s$  or transmembrane potential also results in the change of the membranes' mean curvature (Petrov, 2001) due to the converse flexoelectric effect. Experimentally, this converse flexoelectric effect has been observed using an atomic force microscope (AFM) to measure the deformation of a biomembrane (Mosbacher et al., 1998; Zhang et al., 2001) and optical tweezers (OT) to pull membrane tethers and measure their force production (Brownell et al., 2010) in response to an applied voltage. The membrane tethers had similar geometry to stereocilia lacking only their actin cores. In particular, it has been experimentally observed that the length of stereocilia changes during current flow (Hakizimana et al., 2012).

In the present work, we attempt to construct a physical model that takes into account the nonlinear dynamics, mechanics and flexoelectricity of the hair bundle. The physical model is constructed based on the following three facts: (1) the rotation of the hair bundle changes the tension of the tip links; (2) the ions channel gates are mechano-sensitive and the change of tip link force therefore impacts the opening state of the gates; (3) the ions flowing through the channel gate can significantly change the voltage of the hair bundle and then alter the shape of the stereocilia due to the flexoelectric effect. Although there are numerous parameters that could affect the performance of the hair bundle, such as: the length of the stereocilia, the spring constant for the tip link, the viscosity of the surrounding fluid, and the channel gate parameters, two parameters that make our model different from others are the intracellular charge density (–which may, potentially, be linked with  $K^+$  and  $Ca^{2+}$  ions) and the biomembrane's bending stiffness; both of which also play a critical role in several other biological contexts. Without fitting any artificial parameters—and using merely the thermodynamically defined properties of biomembranes determined by experiments—the current model shows that the hair bundle indeed runs at the edge of a Hopf-bifurcation for typical values of the intracellular charge density and the membranes bending stiffness. The model also indicates that, as the above two parameters deviate from their normal value, Hopf bifurcation and the active motion of the system is severely suppressed. *In particular, we find that flexoelectricity can be a possible cause for the fast adaption for hair bundle's motility and serve as an essential ingredient for the occurrence of Hopf bifurcation. Through the proposed model, we can quantitatively relate the intracellular cations concentration and the membrane's mechanical properties to the nonlinear dynamic behavior of the hair bundle.*

Recently, Maoiléidigh and Hudspeth have proposed a nonlinear model which combines the somatic motility of outer hair cells and the hair bundle's motility to show that the active process in the cochlea is caused by the Hopf-bifurcation (Maoiléidigh and Hudspeth, 2013; Maoiléidigh and Juicher, 2010). The insights from their work emerge to be crucial to the development of the present work. However, our proposed model is different from these aforementioned works in the following aspects<sup>2</sup>:

<sup>2</sup> The outline of the differences between the present work and prior literature should not be viewed as a criticism of the latter. Our intention is to merely highlight the novel contributions of the present work and the context underpinning our model.

- (1) Maoiléidigh and Hudspeth proposed an adaption spring model that attempts to account for the electromechanical coupling in hair bundles (Maoiléidigh and Hudspeth, 2013; Maoiléidigh and Juicher, 2010). They assume that the adaption spring located right at the ions' channel gate is sensitive to cations (more precisely,  $\text{Ca}^{2+}$ ). As cations flow in the channel and bind to the adaption spring, the spring constant decreases. However, this adaption spring has not been identified by experiments yet. In our model, the electromechanical coupling of hair bundles originates from a well accepted behavior of lipid bilayer membranes, flexoelectric effect, which has been identified both theoretically and experimentally;
- (2) Maoiléidigh and Hudspeth's model combines the motions of outer hair cells and hair bundles. The outer hair cells are thought to be *piezoelectric*. In their model, the  $\text{Ca}^{2+}$  concentration is linked to the dynamics of the hair bundle through the opening probability of ion channels (Choe et al., 1998; Maoiléidigh and Hudspeth, 2013; Maoiléidigh and Juicher, 2010). We have been unable to understand the possible mechanism could lead to piezoelectricity in the outer hair cells or biological membranes in general—the symmetry rules of condensed matter physics would appear to preclude this phenomenon in these structures. In our model, the electromechanical coupling is based on flexoelectricity. Through flexoelectricity, the concentration of  $\text{K}^+$  or  $\text{Ca}^{2+}$  is *qualitatively* related to the dynamics of the system;
- (3) Maoiléidigh and Hudspeth's model, as well as any other existing models, are unable to connect the bending stiffness of biomembranes to the active process in cochlea (Maoiléidigh and Hudspeth, 2013; Maoiléidigh and Juicher, 2010). In our model, which directly incorporates the elasticity of membranes, we can see that the change in the biomembranes bending stiffness should cause the loss of the amplification function. In particular, our model yields contour maps of the combination of membrane bending modulus and intercellular charge density that yields the Hopf bifurcation phenomenology.

Breneman et al. (2009) proposed that flexoelectricity of stereocilia is critical to the hearing. Our present work/model differs from their's in the following respects:

- (1) Breneman, Brownell and Rabbitt's model is linear in terms of hair bundle dynamics (Breneman et al., 2009). The linear nature of the model ensures that Hopf-bifurcation is not predicted. Our model simply utilizes the principles of condensed matter physics and soft matter mechanics to derive a set of nonlinear equations from which Hopf-bifurcation emerges naturally for a range of physically measurable parameters;
- (2) Breneman, Brownell and Rabbitt's model doesn't take into account the activity of mechano-sensitive ions channels (Breneman et al., 2009). The ion flow is treated as a known input to the system. Our model takes into account the highly nonlinear behavior of ion-channels. In our nonlinear model, the ions flow is no longer a given function, but depends on the motion of the stereocilia;
- (3) Breneman, Brownell and Rabbitt's model is able to explain the frequency selectivity of hair bundles. However, for the amplification function and the compressive nonlinearity, their model is not suitable since a nonlinear dynamical model is required for that (Breneman et al., 2009).

The outline of the paper is as follows: in Section 2, we derive the central physical model for the hair bundle dynamics based on thermodynamics and principles of soft matter continuum mechanics. We propose that the phenomenon of membrane flexoelectricity is a key mechanism underpinning membrane electromotility. We perform an analytical linearized stability analysis in Section 3 to understand the stability and the frequency selectivity of the hearing system. To confirm our interpretation of the link between Hopf-bifurcation and flexoelectricity, we perform all-numerical simulations of the derived nonlinear model in Section 4 and finally conclude that the hair bundles do run close to a supercritical Hopf-bifurcation for a broad range of physical parameters. The numerical simulations show that an oscillation that initiates within the limit cycle can be amplified to the limit cycle, while an oscillation that initiates outside the limit cycle is pulled back into the limit cycle. This observation is consistent with the experimental observation of nonlinear compression of the active motion of hair bundles.

## 2. A physical model for the dynamics of hair bundles

Normally, a hair bundle is comprised of dozens to hundreds of stereocilia. Each stereocilia is connected to its shorter and longer neighbors by tip links. Without loss of generality, only four stereocilia are shown in the schematic drawing (Fig. 2(a)) to describe the motion of a hair bundle due to the vibration of its base, the BM. The mass block  $M_{AS}$  located on the top of the longest stereocilia represents the mass of the accessory structure including tectorial membrane (TM) and others. Since the weight of the TM is much larger than that of the hair bundle, we simply ignore the weight of the hair bundle. When the vibration of the BM propagates to the hair bundle, it causes the rotation of the stereocilia. This rotation leads to the increase or decrease of the tip link forces which are proportional to the length changes of the tip links. Subsequently, the changes in tip link forces lead to the opening or closing of ions channel gates in stereocilia. Due to the flow of ion and the flexoelectric effect, the stereocilia's radius and length alter. Thus, in this work, we decompose the motion of each stereocilia into two parts: the rotation around the pivot and the shape change.

In prior works, the tip link force is assumed to be linearly proportional to the tip displacement of the connected stereocilia (Breneman et al., 2009; Choe et al., 1998; Maoiléidigh and Hudspeth, 2013; Nadrowski et al., 2004). In Fig. 2(b), to capture the two motion modes mentioned above, we idealize the stereocilia and propose that while it can stretch and rigidly

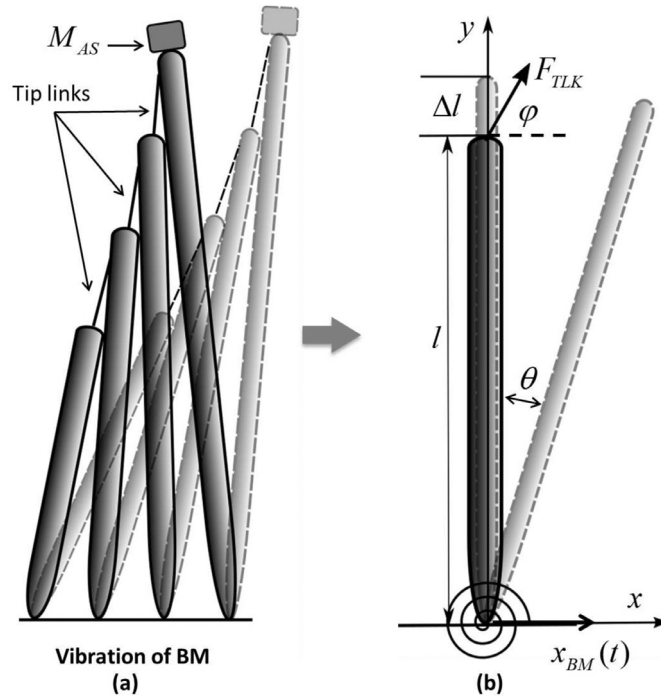


**Fig. 2.** A schematic drawing for the relative motion of a hair bundle. (a) The vibration of a hair bundle in response to the vibration of the BM. Although a hair bundle usually contains dozens to hundreds stereocilia, here, without loss of generality, we only plot four of them to illustrate the central ideas. As the vibration of the BM causes the rotations of stereocilia, the tip links' length will change accordingly. For each tip link, its length change usually leads to a tip link force. (b) An effective model describes the mechanics of a stereocilia. Note that the rotation angle  $\theta$  is caused by external forces including the BM's vibration and the tip link force  $F_{TLK}$ , while the length change  $\Delta l$  is caused by the flexoelectricity of the stereocilia. The tip link force  $F_{TLK}$  is along the tip link.

rotate (as shown), it does not “bend” along the longitudinal direction. These simplifications, while approximations, are fairly well-grounded, based on the phenomenology of the problem. Experimental observations appear to indicate, also shown in Fig. 2(a), that each stereocilia becomes thinner at the region close to its root. Thus, the stereocilia is more likely to pivot about its root than bend into a curve shape. We remark that the stretch and rotation modes interact with each other during the vibration of a stereocilia and form a highly coupled system. The length change  $\Delta l$  (corresponding to the stretching mode) of a stereocilia can make the connected tip links change their length and subsequently result in the change of the tip link force  $F_{TLK}$ . As shown in Fig. 2(b),  $F_{TLK}$  along with the BM vibration affects the rotation of the stereocilia. The rotation of the stereocilia, in turn, can also change the magnitude of the tip link force and subsequently lead to the change of the ion channel opening state. Opening and closure of the ion channels then changes the stereocilia radius ( $R$ ) due to the flexoelectric effect. Finally,  $\Delta l$  is related to  $R$ , through appropriate geometrical and physical constraints, to stereocilia's shape change (as will be evident shortly).

There are several factors that may cause a shape change of the stereocilia. Firstly, the pressure difference between the inner and the outer walls of the stereocilia can potentially cause a change of shape. Secondly, the fluid inside the stereocilia makes it difficult for the total volume to change in a short time (several ms). Thus, in the analysis of high frequency vibration, it is reasonable to assume that the volume enclosed by the stereocilia is conserved which implies that the changes in the radius  $R$  and the length  $l$  are coupled by

$$V(t) = \pi R(t)^2 l(t) = V_0 = \pi R_0^2 l_0, \quad (2.3)$$

where  $l_0$  and  $R_0$  respectively denote its initial length and the radius. So the length change  $\Delta l$  can be expressed in term of the radius as

$$\Delta l = l - l_0 = \left( \frac{R_0^2}{R^2} - 1 \right) l_0. \quad (2.4)$$

Finally, the shape of the stereocilia is also affected by its voltage difference between the inner and outer walls through flexoelectricity. In this work, we propose that this is the main reason for the active motion of the stereocilia since it can keep transferring ions flow into mechanical vibration and supply energy to compensate what has been dissipated by the surrounding fluid.

## 2.1. Rotation mode of the stereocilia

We first address the rotation mode of the stereocilia shown in Fig. 2(b). We denote the relative displacement of the stereocilia tip to its base, the BM, by  $x$  and the base displacement by  $x_{BM}$ . Due to the rotational spring located at the base of the stereocilia, the rotation angle  $\theta$  is proportional to the total moment by a factor  $K_{rsp}$  which is the spring constant. Assuming that the rotation angle  $\theta$  is always very small, the motion of the stretchable bar is governed by the following equation:

$$K_{rsp}\theta = K_{rsp}\frac{x}{l_0} = [F_{tip}\cos\varphi - M_{AS}(\ddot{x} + \ddot{x}_{BM}) - c_{eff}(\dot{x} + \dot{x}_{BM})]l_0, \quad (2.5)$$

where  $c_{eff}$  is the effective damping coefficient and  $K_{rsp}$  is the spring constant of the rotational spring.  $F_{tip}$  is the tip link force applied from the tip link to the stereocilia. The tip link force is in the direction of the tip link and proportional to the length change of it. Without loss of generality, we assume that the length change of a tip link is proportional to both  $x$  and  $\Delta l$ . Thus, the tip link force may be given by

$$F_{tip} = K_L(x\cos\varphi - \Delta l\sin\varphi), \quad (2.6)$$

where  $K_L$  is the effective tip link spring constant which links the tip displacement to the tip link force. In Eq. (2.6), the negative sign is an indication that the effects of  $x$  and  $\Delta l$  are opposite to each other.

Substituting (2.6) into (2.5) and after some manipulations, we arrive at the following equation for the motion of a stereocilia (in terms of the two unknowns  $x$  and  $\Delta l$ ):

$$M_{AS}\ddot{x} + c_{eff}\dot{x} + (K_{eff} - K_L\cos^2\varphi)x = -K_L\sin\varphi\cos\varphi\Delta l + F_{stim}, \quad (2.7)$$

where

$$K_{eff} = \frac{K_{rsp}}{l_0^2} \quad (2.8)$$

is defined as an effective spring constant which links the tip displacement  $x$  to the force applied on it. As shown in Eq. (2.8),  $K_{eff}$  is inversely proportional to  $l_0^2$ . Longer stereocilia (larger  $l_0$ ) leads to smaller  $K_{eff}$  and subsequently lower natural frequency. Thus, for a fixed  $l_0$ ,  $K_{eff}$  is treated as a constant.

$$F_{stim} = -M_{AS}\ddot{x}_{BM} - c_{eff}\dot{x}_{BM} \quad (2.9)$$

is the effective stimulation force due to the vibration of the BM. This stimulation force can also be regarded as an input to the system. This input comes from the sound heard by our ears. An additional equation is required to resolve both  $x$  and  $\Delta l$  which is tied to the electro-mechanical coupling exhibited by the system.

## 2.2. Flexoelectricity induced deformation of the stereocilia

Other than the rotation motion mode, the stereocilia can also change its shape in response to mechanical and electrical stimulations. In the following, we formulate flexoelectricity and deformation of the stereocilia through Hamilton's principle. We remark that the general topic of flexoelectricity has generated significant recent interest in the mechanics community in a variety of contexts ranging from materials design to energy harvesting (Abdollahi et al., 2015; Catalan et al., 2010; Chandratre and Sharma, 2012; Cross, 2006; Deng et al., 2014a,b; Dumitrica et al., 2002; Kothari et al., 2018; 2019; Liu and Sharma, 2013; Mao and Purohit, 2015; Maranganti et al., 2006; Nanthakumar et al., 2017; Rahmati et al., 2019; Zhou et al., 2018). The reader is referred to the following works for an overview of the subject (Ahmadpoor and Sharma, 2015; Deng et al., 2016; Krichen and Sharma, 2016; Nguyen et al., 2013; Yudin and Tagantsev, 2013; Zubko et al., 2013).

### 2.2.1. Deformation pattern of the stereocilia

The stereocilia are usually very long compared to its diameter so it is appropriate to model them as cylindrical shells—ignoring thus any end effects. To simplify matters further, also assume that the deformation of the cylindrical shell is always uniform and the thickness of the membrane ( $h$ ) does not change with its deformation. Thus the shape of a stereocilia is confined to be cylindrical throughout the deformation and its mean curvature  $H(t)$  at time  $t$  is simply the reciprocal of the radius  $R(t)$ . For the specific case considered here, the displacement in the radial direction ( $w$ ) is uniform and related to  $R(t)$  by

$$w(t) = R(t) - R_0, \quad (2.10)$$

where  $R_0$  denotes the radius of the undeformed stereocilia. The longitudinal change of the stereocilia can be described by the displacement ( $u$ ) which is in the longitudinal direction and linear with respect to the longitudinal coordinate  $y$  so that the deformation in this direction is uniform. Let the displacement  $u(y, t)$  at  $y = 0$  be zero, then we have

$$u(y, t) = \left(\frac{l(t)}{l_0} - 1\right)y. \quad (2.11)$$

The objectives of (2.10) and (2.11) are to convert two field variables  $w(t)$  and  $u(t)$  into two state variables  $R(t)$  and  $l(t)$ . With these two state variables, the deformed configuration of a stereocilia can be determined.

2.2.2. Hamilton’s principle for the stereocilia

The dissipation of a fluctuating lipid membrane in viscous fluid is complex but relatively reasonable way to handle that is to take the energy dissipation rate as proportional to the bending and torsion rates,  $Q^B$  and  $Q^T$ . Here, we should distinguish the bending of membranes’ from the bending of the stereocilia. In the preceding section, we assumed that the stereocilia does not bend. However, the membrane that makes up the stereocilia can bend (or wrap up) into a cylindrical shape. Following Rey’s approach (Rey, 2008), the dissipation bending moment  $\mathcal{M}^B$  and torsion moment  $\mathcal{M}^T$  are defined as:

$$\mathcal{M}^B = c^B Q^B \tag{2.12}$$

$$\mathcal{M}^T = c^T Q^T, \tag{2.13}$$

where  $c^B$  and  $c^T$  are the bending and torsion viscosities. Consider a fluctuating membrane whose middle plane denoted by  $\omega$ . We may then derive its electromechanical behavior through recourse to Hamilton’s principle given by:

$$\delta \int_{t_0}^{t_1} dt \left\{ \int_{\omega} \left[ \frac{h}{2} \rho (\dot{u}^2 + \dot{w}^2) - \mathcal{H} \right] da - \lambda (V - V_0) \right\} + \int_{t_0}^{t_1} dt \left[ \int_{\omega^\pm} t^e \delta w da - \int_{\omega^\pm} \bar{q} \delta \phi da - h \int_{\omega} \mathcal{M} \delta H da \right] = 0, \tag{2.14}$$

where  $\delta^{(*)}$  denotes the variation of a functional,  $\rho$  is the mass density,  $V = \pi R^2 l$  is the volume enclosed by the cylindrical membrane whose length and radius are respectively denoted by  $l$  and  $R$ , the Lagrangian multiplier  $\lambda$  is used to ensure that the total volume  $V$  does not change the deformation,  $V_0$  is the initial value for  $V$ ,  $\omega^+$  and  $\omega^-$  denote the outer and inner surfaces of the membrane, respectively. The external pressure applied normal to the surfaces  $\omega^\pm$  by the surrounding fluid is denoted by  $t^e$ . The density of the net charges attached to the surfaces  $\omega^\pm$  is  $\bar{q}$  and  $\phi$  is the electric potential. The last term in (2.14) corresponds to the energy dissipation due to viscous damping. The energy dissipation part is simply written as  $\mathcal{M} \delta H$  where  $\mathcal{M} = c \dot{H}$  is the effective moment and  $c$  is the effective viscosity that links the mean curvature  $H$  to  $\mathcal{M}$ .

For the pure mechanical problem,  $\mathcal{H}$  is taken as internal energy density of the system. For the electromechanical coupling problem described here,  $\mathcal{H}$  is given by

$$\mathcal{H} = W(H, K, \Pi) - e \cdot (p_s + p^e) - \frac{h \epsilon_0}{2} e^2, \tag{2.15}$$

where  $K$  designates the Gaussian curvature which, due to the celebrated Gauss-Bonnet theorem, is irrelevant in our context. The symbol  $e$  is the electric field and  $\epsilon_0$  is the vacuum permittivity. Here, we also consider the contribution from the external polarization  $p^e$  which might be caused by proteins embedded in the membrane. Since  $p^e$  represents the polarization density per unit area and the surface area of a membrane changes with its deformation,  $p^e$  relates to its original value  $P_0^e$  in the undeformed state by

$$p^e da = P_0^e dA \tag{2.16}$$

where  $da$  and  $dA$  denote the area of a small part of the membrane in its deformed and undeformed states, respectively. Note that  $P_0^e$  is a fixed parameter which only depends on the initial conformation of the membrane but not on the deformation of it. In order to decouple the dependence of the polarization  $p_s$  on the local deformation of the membrane, we introduce  $\Pi$ , the mass density of polarization, which is related to  $p_s$  by

$$\Pi = \frac{p_s}{h \rho}. \tag{2.17}$$

A quadratic form for the internal energy density  $W$  may be written as

$$W = \frac{1}{2} \kappa_b H^2 + \frac{1}{2} a p_s^2 + f H p_s, \tag{2.18}$$

where  $\kappa_b$  is the bending modulus,  $f$  is the constant for flexoelectricity and the coefficient  $a = 1/((\epsilon_r - 1)\epsilon_0 h)$  links the polarization to the internal energy density. Note that  $f$  is different from but related to the flexoelectric coefficient  $\mu$  in Eq. (1.1) by  $f = -a\mu$ .

Notice that  $\omega$  and  $\omega^\pm$  respectively denote the middle layer and the surface layers of the biomembrane in its deformed state. So the integration domains in (2.14) change with time. For the convenience of variational calculus, we firstly convert domains  $\omega$  and  $\omega^\pm$  into their counterparts in the undeformed or reference state. Here, we denote the undeformed middle layer and the surface layers by  $\Omega$  and  $\Omega^\pm$ , respectively. In this work, the thickness  $h$  is assumed to be constant and the ratio of  $\omega$  to  $\Omega$  is  $J = \frac{Rl}{R_0 l_0}$  due to the uniform deformation assumption. Correspondingly, the four governing equations may be obtained through the usual variational calculus procedure given below:

(1) Variation of the kinetic energy

During deformation, the stereocilia changes its radius and length with time. Thus, the kinetic energy contains two parts corresponding to the displacement  $u(t)$  and  $w(t)$ . Assuming that the mass density is a constant throughout the

whole membrane prior to deformation, the kinetic energy can be written as:

$$\delta \int_{t_0}^{t_1} dt \left[ \int_{\omega} \frac{h}{2} \rho (\dot{u}^2 + \dot{w}^2) da \right] = \int_{t_0}^{t_1} dt \left[ \int_{\Omega} -\rho_0 h (\ddot{u} \delta u + \ddot{w} \delta w) dA \right], \tag{2.19}$$

where  $\rho_0$  is the mass density of the undeformed membrane. Because of the local mass conservation and constant thickness assumption, we have  $\rho da = \rho_0 dA$ .

(2) **Variation of the internal energy**

The internal energy is an integral of the internal energy density  $W(H, K, \Pi)$ . Thus, its variation is given by

$$\begin{aligned} \delta \int_{t_0}^{t_1} dt \int_{\omega} W(H, K, \Pi) da &= \int_{t_0}^{t_1} dt \int_{\Omega} (\delta W J + W \delta J) da \\ &= \int_{t_0}^{t_1} dt \int_{\Omega} [(W_H \delta H + W_{\Pi} \delta \Pi) J + W \delta J] dA, \end{aligned} \tag{2.20}$$

where  $W_H$  and  $W_{\Pi}$  denote the derivatives of the energy density function  $W$  with respect to the mean curvature  $H$  and the polarization  $\Pi$ , respectively. The variation of  $J$  is given by

$$\delta J = \frac{R}{R_0 l_0} \delta l + \frac{l}{R_0 l_0} \delta R. \tag{2.21}$$

(3) **Variation of the energy associated with the electric field**

Due to the assumption of constant electric field across the thickness of the membrane, the electric field can be simply expressed as

$$e = -\frac{\Delta \phi}{h}.$$

So the variation of the energy associated with the electric field becomes

$$\begin{aligned} \delta \int_{t_0}^{t_1} dt \left\{ \int_{\omega} \left[ e(p_s + p^e) + \frac{h \epsilon_0}{2} e^2 \right] da \right\} \\ = \delta \int_{t_0}^{t_1} dt \int_{\Omega} \left[ -\Delta \phi (\rho_0 \Pi + \frac{P_0^e}{h}) + \frac{\epsilon_0}{2h} (\Delta \phi)^2 J \right] dA \\ = \int_{t_0}^{t_1} dt \int_{\Omega} \left[ -\Delta \phi \rho_0 \delta \Pi + \left( \frac{\epsilon_0}{h} \Delta \phi J - \rho_0 \Pi - \frac{P_0^e}{h} \right) \delta (\Delta \phi) + \frac{\epsilon_0}{2h} (\Delta \phi)^2 \delta J \right] dA, \end{aligned} \tag{2.22}$$

where  $\Delta \phi = \phi^+ - \phi^-$  denotes the potential difference between the surfaces  $\omega^+$  and  $\omega^-$ .

(4) **Virtual work done by the mechanical forces**

We denote the external pressure applied to the surfaces  $\omega^+$  and  $\omega^-$  by  $t^{e+}$  and  $t^{e-}$ , respectively. Since the membrane is very thin and assumed to have constant thickness, it is reasonable to assume that the displacement  $w$  is constant across the thickness of the membrane. So we have

$$\int_{\omega^{\pm}} t^{e\pm} \delta w da = \int_{\omega} \Delta t^e \delta w da = \int_{\Omega} \Delta t^e \delta w J dA, \tag{2.23}$$

where  $\Delta t^e = t^{e+} - t^{e-}$  represents the pressure difference between the two surfaces  $\omega^+$  and  $\omega^-$ .

(5) **Virtual work done associated with the surface charges attached to  $\omega^{\pm}$**

Normally, the charge density of a lipid bilayer membrane surfaces is negative due to the arrangement of its lipid molecules. The emergent or coarse-grained or continuum parameters representing the dielectric constant and flexoelectric coefficient dictate the electromechanical behavior of the membrane. These intrinsic surface charges endow the membrane with flexoelectricity. Thus, the lipid bilayer membrane can be viewed as a flexoelectric thin membrane without surface intrinsic charges. In this work, we follow this idea and employ a flexoelectric membrane model to account for the intrinsic surface charge of the lipid bilayer membrane. In reality, there are also ions moving towards and binding with the membrane. They can effectively alter the potential of the membrane and affect its electromechanical behaviors. It is worthwhile to mention that the charge densities appear in the following equations are those due to the moving ions.

$$\int_{\omega^{\pm}} \bar{q} \delta \phi da = \int_{\omega} (q^+ \delta \phi^+ + q^- \delta \phi^-) da = \int_{\Omega} (q^+ \delta \phi^+ + q^- \delta \phi^-) J dA, \tag{2.24}$$

where  $q^+(t)$  and  $q^-(t)$  represent the charge densities on surfaces  $\omega^+$  and  $\omega^-$ , respectively. Note that these charge densities are due to the ions exist in the electrolyte surrounding and within the stereocilia. The variation of potential  $\phi$  on these two surfaces are denoted by  $\delta \phi^+$  and  $\delta \phi^-$ . Usually, the charge density in the external electrolyte is relatively stable. So the change of the charge density and potential on the outer surface  $\omega^+$  is much slower than the inner surface. Accordingly, we simply assume that  $q^+$  and  $\phi^+$  are constants when the stereocilia is vibrating. Thus the term  $q^+ \delta \phi^+$  in (2.24) is zero.

Power and coworkers proposed that the stretch force that arise in tip links influence the channel of the stereocilia (Power et al., 2014; 2012). Thus, in this work, we assume that the inner surface charge density  $q^-$  depends on the  $K^+$  and  $Ca^{2+}$  ions flowing through the mechano-sensitive ion channels. Experiments indicates that the current associated with the ions flowing relates to the hair bundle’s deflection by Fettiplace and Kim (2014)

$$I = I_{max}/\{1 + \exp[(x_0 - x)/x_s]\},$$

where  $I_{max}$  is the peak value of the current  $I$ ,  $x$  is the deflection,  $x_0$  is the deflection to half activate the current, and  $x_s$  is the slope factor which determines how fast the ion channel opening state is switched with respect respect to the hair bundle deflection. Thus the expression for ion channel open probability  $P_0$  can be proposed as:

$$P_0 = 1/\{1 + \exp[(x_0 - x)/\Delta]\}, \tag{2.25}$$

where the parameter  $\Delta$  denotes the range of the hair bundle deflection over which the channel open probability changes from 10% to 90%. Without loss of generality, in this work, we set  $x_0 = 0$  for simplicity.

We designate the positive charge density of the inner surface of the stereocilia with opening ions channels as  $q_0$ . As the channel open probability decreases, fewer positive charged ions, such as:  $K^+$  or  $Ca^{2+}$ , flow inside the stereocilia and cause the decrease of the value of  $q_0$ . The inner surface charge density  $q^-$  for a specific  $P_0$  is given by

$$q^- = \alpha P_0 q_0, \tag{2.26}$$

where  $\alpha$  is a parameter less than 1 and describes the sensitivity of channel opening. When the channel is closed,  $P_0 = 0$  and  $q^- = 0$ . While if the channel is open,  $P_0 = 1$  and  $q^- = \alpha q_0$ .

(6) **Virtual work done by the dissipative moment  $\mathcal{M}$**

The virtual work done by the dissipative moment is given by the last term of (2.14). With  $\mathcal{M} = c\dot{H}$ , then we have

$$\int_{\omega} \mathcal{M} \delta H da = \int_{\omega} c \dot{H} \delta H da = \int_{\Omega} \frac{c}{R^4} \dot{R} \delta R J dA. \tag{2.27}$$

Substituting (2.19)–(2.27) into (2.14) and keep in mind that the Lagrange multiplier  $\lambda$  is an unknown, we obtain:

$$\begin{cases} -\frac{2Wl}{R_0 l_0} + \frac{\epsilon_0 l (\Delta\phi)^2}{R_0 l_0 h} - J\lambda = \frac{2}{3} \frac{\rho_0 h l}{R} \ddot{l} \\ \frac{JW_{\dot{H}}}{R^2} - \frac{Wl}{R_0 l_0} + \frac{\epsilon_0 l (\Delta\phi)^2}{2R_0 l_0 h} + \Delta t^e J + \frac{\mathcal{M} J h}{R^2} - J\lambda = \rho_0 h \ddot{R} \\ \rho_0 \Delta\phi + JW_{\Pi} = 0 \\ \frac{\epsilon_0}{h} \Delta\phi J - \rho_0 \Pi + (q^- - \frac{p^e}{h}) J = 0. \end{cases} \tag{2.28}$$

Note that from the 4th equation of (2.28), we may find that the effect of external polarization  $p^e$  is just like the surface charge  $q^-$ . Here, we introduce  $q^-_{eff} = q^- - \frac{p^e}{h}$  to represent the effective surface charge density. In what follows, we ignore external polarization since its contribution can be equivalently introduced by appropriately adjusting the charge density  $q^-$ .

2.2.3. *Nonlinear governing equation for the radius  $R(t)$*

Substituting (2.18) into the third and fourth equations of (2.28) and keeping in mind that  $H = 1/R$ , we obtain

$$\begin{cases} \Pi = -\frac{f\epsilon_0}{R\eta\rho h} + \frac{q^-}{\eta\rho h} \\ \Delta\phi = -\frac{ahq^-}{\eta} - \frac{f}{\eta R}, \end{cases} \tag{2.29}$$

where  $\eta = a\epsilon_0 + \frac{1}{h}$ .

The constant volume constraint (2.3) can be rewritten as

$$l = R_0^2 l_0 / R^2. \tag{2.30}$$

Applying the first and the second time derivatives to (2.30), we have

$$\dot{l} = -2 \frac{R_0^2 l_0}{R^3} \dot{R} \tag{2.31}$$

and

$$\ddot{l} = 6 \frac{R_0^2 l_0}{R^4} (\dot{R})^2 - 2 \frac{R_0^2 l_0}{R^3} \ddot{R}. \tag{2.32}$$

Using (2.29)–(2.32) along with the first equation of (2.28), we may eliminate the variables  $\Pi$ ,  $\Delta\phi$ ,  $l$  and  $\lambda$  in the second equation of (2.28) and finally obtain a nonlinear governing equation for  $R$ ,

$$\begin{aligned} \rho_0 h \left( \frac{R^5}{R_0} + \frac{4}{3} \frac{R_0^3 l_0^2}{R} \right) \ddot{R} - 4 \frac{\rho_0 h R_0^3 l_0^2}{R^2} (\dot{R})^2 + ch\dot{R} - \left[ \frac{3}{2} \kappa_b - \frac{f^2 \epsilon_0}{\eta} \left( \frac{3}{2} + \frac{1}{\eta h} \right) \right] R - 2 \frac{f q^-(x)}{h \eta^2} R^2 \\ + \frac{a(a\epsilon_0 h - 1)}{2\eta^2} (q^-(x))^2 R^3 = \Delta t^e R^4, \end{aligned} \tag{2.33}$$

where the expression for  $q^-(x)$  is given by (2.26).

Since the total volume of the stereocilia is conserved, this means there is no net fluid flow inside or outside the stereocilia. A further implication is that the shape change of the stereocilia is mainly due to the flexoelectric effect, but not the pressure difference between the two sides of the lipid bilayer membrane. For this reason, the pressure difference  $\Delta t^e$  can be considered to be unchanged during the whole process. By setting  $R = R_0$ ,  $\dot{R} = 0$  and  $x = 0$ , we may obtain the following expression for  $\Delta t^e$ :

$$\Delta t^e = - \left[ \frac{3\kappa_b}{2} - \frac{f^2\epsilon_0}{\eta} \left( \frac{3}{2} + \frac{1}{\eta h} \right) \right] \frac{1}{R_0^3} - \frac{\alpha f q_0}{\eta^2 h R_0^2} - \frac{a(1 - a\epsilon_0 h)\alpha^2 q_0^2}{8\eta^2 R_0}. \quad (2.34)$$

It is known that the high frequency vibration in a viscous fluid is usually over damped. Since the vibration frequency we are interested in is over several kHz and the surrounding fluid is very viscous, it is reasonable to assume that the system is over damped and we can ignore the contribution of the kinetic energy in (2.14). Thus, (2.33) may be simplified as

$$ch\dot{R} - \left[ \frac{3}{2}\kappa_b - \frac{f^2\epsilon_0}{\eta} \left( \frac{3}{2} + \frac{1}{\eta h} \right) \right] R - 2 \frac{f q^-(x)}{h\eta^2} R^2 + \frac{a(a\epsilon_0 h - 1)}{2\eta^2} (q^-(x))^2 R^3 = \Delta t^e R^4. \quad (2.35)$$

If we further assume that the shape change of the stereocilia is not large, the Maxwell stress effect may be also ignored. So (2.35) can be further simplified as

$$ch\dot{R} = \left( \kappa_b - \frac{f^2\epsilon_0}{\eta} \right) R + \frac{f q^-(x)}{\eta} R^2 + \Delta t^e R^4, \quad (2.36)$$

and the term  $\Delta t^e$  may be also reduced to

$$\Delta t^e = - \left( \kappa_b - \frac{f^2\epsilon_0}{\eta} \right) \frac{1}{R_0^3} - \frac{\alpha f q_0}{2\eta R_0^2}. \quad (2.37)$$

Eqs. (2.7) and (2.36) can be combined to solve for the two variables  $x(t)$  and  $R(t)$ . With  $R(t)$  determined, the variable  $l(t)$  can be obtained using the constant volume Eq. (2.3), the constant volume constraint.  $\Pi(t)$  and  $\Delta\phi(t)$  can be calculated based on  $R(t)$  through Eq. (2.29).

### 3. Sharp frequency selectivity of hair bundles due to flexoelectricity

In the previous section, we introduced two different modes of motion for the hair-bundles: rotation and shape change. These two modes are coupled to each other by tip-link forces and the flexoelectric effect of the biomembrane. As the force in a tip-link is changed by a small vibration, that also causes a change of the state (open probability) of the surrounding ion channels. If the ion channel is open, more cations flow inside the stereocilia and subsequently alter its voltage. Due to the converse flexoelectric effect, the voltage change across the lipid bilayer membrane may lead to a change in its curvature. So the stereocilia experiences a shape change in response to the opening of its ion channels. According to (2.6), the tip-link force also depends on the length change  $\Delta l$  of the stereocilia. Thus, the tip-link force and the length change  $\Delta l$  interact with each other during the vibration of the stereocilia.

One of the main objectives of this section is to study how the cations' flow modulates an active motion of the stereocilia through the flexoelectric effect. To begin with, we choose the parameters according to references (Breneman et al., 2009; Maoileidigh and Hudspeth, 2013; Petrov, 2001; 2006; Rey, 2008). As an ideal model for the ions channel gate, we set  $\alpha = 1$  which means that the channel can be completely open or closed according to the tip-link force. The parameters  $q_0$  and  $\kappa_b$  are set to their normal values initially. In the later analysis, we will alter these values within a reasonable range to examine the sensitivity of the system's dynamical behavior to these choices.

For the system governed by (2.7) and (2.36), we anticipate that the effect of  $\kappa_b$  is significant due to nonlinearities. Another parameter of interest is the initial charge density  $q_0$  of a stereocilia's inner surface which largely depends on the cations' density of the surrounding electrolyte<sup>3</sup> Accordingly, we vary  $\kappa_b$  and  $q_0$  separately and study how the dynamical behavior of the system changes as a result. The rationale for choosing these two parameters is that a variety of environmental causes may alter these in mammalian or human body e.g. diseases, medicines, or temperature. Using the proposed theoretical model, we aim to set the basis to link the human hearing ability to the above mentioned conditions.

Initially, before the application of external stimulations, the stereocilia is at its equilibrium state (stationary point) where the time derivatives of  $x$  and  $R$  are both zero. The stationary point  $(x^s, R^s)$  can be solved from (2.7) and (2.36) by setting  $\ddot{x} = \dot{x} = \dot{R} = 0$ . In Fig. 3, we plot curves for Eqs. (2.7) and (2.36) with  $\ddot{x} = \dot{x} = \dot{R} = 0$ . Each color corresponds to a choice of  $\kappa_b$  and  $q_0$ . It's seen from the figure that, for different combinations of  $\kappa_b$  and  $q_0$ , the stationary point remains at  $(x^s = 0, R^s = R_0)$ . So we conclude that the position of the stationary point is independent of the choice of  $\kappa_b$  and  $q_0$ . This conclusion ensures that the subsequent studies need be performed using only a single stationary point.

<sup>3</sup> Theoretically, the surface charge density is less than several tens of  $mC/m^2$  depending on the concentration of the cations in the surrounding environment, the density of the binding sites in the membrane, and the binding energy of the binding site to cations (Lakshminarayana, 1977). Here, since the gate opening time is very short for each cycle of the vibration, we choose a relatively small nominal value of  $q_0$ .

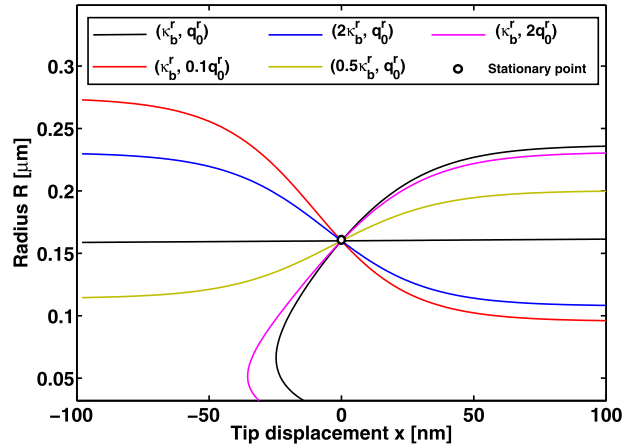


**Fig. 3.** Stationary point for different combinations of  $\kappa_b$  and  $q_0$ . All curves intersect at the same point, which implies that the stationary point ( $x^s$ ,  $R^s$ ) is insensitive to the parameters  $\kappa_b$  and  $q_0$ . Note  $\kappa_b^r = 20k_B T$  and  $q_0^r = 0.2mC/m^2$  denote the reference values for the parameters  $\kappa_b$  and  $q_0$ .

**Table 1**  
Parameters for the rotation physics pertaining to the hair bundle.

Symbol	Values	Symbol	Values
$M_{AS}$ (ng)	32	$\kappa_b$ (J)	$30k_B T$
$c_{eff}$ (nN · s · m <sup>-1</sup> )	150	$\epsilon_r$	30
$K_{eff}$ (mN · m <sup>-1</sup> )	4.5	$\rho$ (kg/m <sup>3</sup> )	1000
$K_L$ (mN · m <sup>-1</sup> )	4.5	$c$ (N · m · s)	$10^{-15}$
$R_0$ (μm)	0.16	$h$ (nm)	5
$l_0$ (μm)	6	$\Delta$ (nm)	20
$\varphi$	$\pi/4$	$\mu$ (C)	$1 \times 10^{-19}$
$q_0$ (mC/m <sup>2</sup> )	0.2	$\alpha$	1(ideal model)

Linearizing the system at the stationary point may provide us some general ideas of the dynamics of the system. Based on the stationary point found above, the linearized version of the system of Eqs. (2.7) and (2.36) is:

$$\begin{bmatrix} \dot{x} \\ \dot{v} \\ \dot{R} \end{bmatrix} = \begin{bmatrix} 0 & 1 & 0 \\ K_1 & K_2 & K_3 \\ K_4 & 0 & K_5 \end{bmatrix} \begin{bmatrix} x \\ v \\ R - R_0 \end{bmatrix} + \begin{bmatrix} 0 \\ F_{stim}/M_{AS} \\ 0 \end{bmatrix} \quad (3.38)$$

where  $v = \dot{x}$  is the hair bundle's tip velocity,  $K_1 = -\frac{K_{eff} - K_L/2}{M_{AS}}$ ,  $K_2 = -\frac{c_{eff}}{M_{AS}}$ ,  $K_3 = \frac{K_L l_0}{R_0 M_{AS}}$ ,  $K_4 = \frac{f q_0 R_0^2}{4\eta h c \Delta}$ , and  $K_5 = \frac{\kappa_b - \frac{f^2 \epsilon_0}{\eta}}{hc} + (4\Delta t^e R_0^3 + \frac{f q_0 R_0}{\eta})/(hc)$ .

Suppose the external stimulation  $F_{stim}$  is harmonic, i.e.  $F_{stim} = F_0 e^{i\omega t}$  with  $\omega$  being the angular frequency, then for the linearized system (3.38), the responses  $x(t)$  and  $R(t)$  are both harmonic such that,  $x(t) = A e^{i\omega t}$  and  $R(t) = R_0 + B e^{i\omega t}$ . Substituting the above expressions for  $F$ ,  $x$  and  $R$  into (3.38) and solving for the amplitude  $A$  for the variable  $x$ , we have

$$A(\omega) = \frac{-F_0}{M_{AS}(\omega^2 + K_1 + iK_2 + \frac{K_3 K_4}{i\omega - K_5})}. \quad (3.39)$$

Obviously,  $A$  is a function of the angular frequency  $\omega$  and also depends on multiple parameters. To study the frequency dependence of  $A$ , we use the parameters given in Table 1. To simulate a small acoustic stimulation,  $F_0$  is chosen to be 1pN. Fig. 4 shows the comparison of the frequency dependency of  $A$  for the cases with and without flexoelectricity. As shown in Fig. 4, the resonance frequency of the linear system changes from 1276Hz to 3178Hz due to the consideration of flexoelectricity. This result indicates that flexoelectricity allows the system to resonant at higher frequencies. Fig. 4 also shows that, if we normalize  $A$  by its value at low frequency where  $A(\omega) = A_0$  is almost a constant, the curve with flexoelectricity exhibits a much sharper peak around the resonance frequency than that for the case without flexoelectricity. This implies that the stereocilia may utilize flexoelectricity to enhance its frequency selection performance. In the plot of Fig. 4, we consider three cases to show how does flexoelectricity affect the frequency selectivity of the system. It is found that the case for  $\kappa_b = 30k_B T$  and  $q_0 = 0.2mC/m^2$  shows the best frequency selectivity among the others. Later, we will show that  $\kappa_b = 30k_B T$  and  $q_0 = 0.2mC/m^2$  correspond to a special situation at which the system runs at the verge of the Hopf-bifurcation. Thus, we may also conclude that the Hopf-bifurcation helps to enhance the frequency selectivity.

It is worthwhile to mention that the frequency response derived from our flexoelectric approach (Fig. 4) differs qualitatively from that obtained in prior works e.g. Hudspeth et al. (2010). The latter is symmetrical about the resonance frequency.

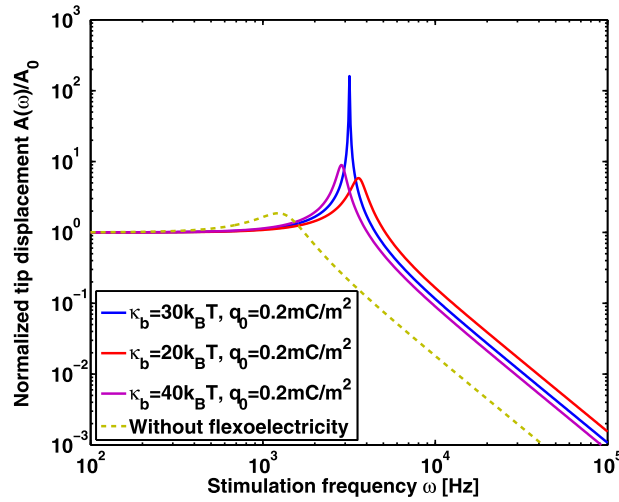


Fig. 4. The frequency dependence of  $A$  for the cases of with and without flexoelectricity. The blue line corresponds to the case of with flexoelectricity has sharper peak which indicates that flexoelectricity enhances the frequency selection. (For interpretation of the references to colour in this figure legend, the reader is referred to the web version of this article.)

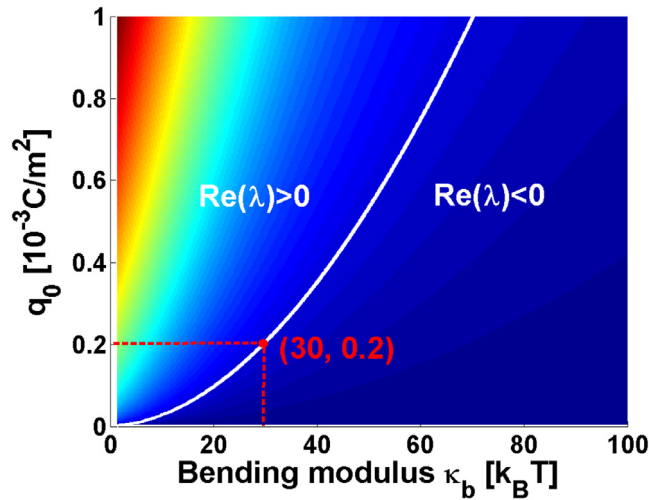


Fig. 5. The change of real part of the complex conjugate eigenvalues with respect to  $\kappa_b$  and  $q_0$ .

In contrast, our flexoelectric bundle frequency response is low pass below the resonance frequency and has an abrupt roll off above. The low pass below and abrupt roll off above the resonance frequency resembles the frequency response we obtained for a model of the outer hair cell lateral wall as a thin, compliant cylindrical piezoelectric (Weitzel et al., 2003). The high frequency roll off is consistent with classical and contemporary measurements of the cochlear traveling wave. Recent cochlear mechanics studies (Cooper et al., 2018; Dewey et al., 2019) have revealed the presence of low frequency amplification at frequencies several octaves below the presumed resonance frequency. The low pass behavior in our model is consistent with electromechanical amplification occurring at frequencies well below the resonance frequency.

We also note that, in the discussed linearized case, the actual values for  $A$  are very small (less than  $1\text{nm}$ ). However, in reality, the response of a stereocilia is much larger due to a process of amplification. It is expected that the amplification probably stems from a Hopf-bifurcation related active motion of the stereocilia. Next, we explore this aspect—i.e. the response of a stereocilia to a small perturbation.

Firstly, we calculate the eigenvalues of the system to check its stability and predict how it behaves when losing stability. Normally, there are three eigenvalues for (3.38). With the parameters given by Table 1, it is found that two of the eigenvalues are a pair of complex conjugates whose real parts ( $Re(\lambda)$ ) are positive. We also find that varying the values of  $\kappa_b$  and  $q_0$  alters the values of  $Re(\lambda)$ .

In Fig. 5, we plot the real part of the conjugate pair  $Re(\lambda)$  as a function of the parameters  $\kappa_b$  and  $q_0$ . The white line in the figure represents the condition under which  $Re(\lambda)$  becomes zero. This white line corresponds to the supercritical

Hopf-bifurcation points of the system. As shown in Fig. 5, on the right hand side of the white line,  $Re(\lambda)$  is less than zero which implies that the vibration of the system is stable. While on the left hand side of the white line,  $Re(\lambda)$  is greater than zero which implies that the vibration of the system is unstable. Since the imaginary part of  $\lambda$  is basically nonzero, when  $Re(\lambda) > 0$ , the system has a limit cycle whose radius may be determined by the parameters  $\kappa_b$  and  $q_0$ . If the radius of this limit cycle is large enough, the system may act as an amplifier that transforms a small input stimulation vibration into a larger one.

Starting from the region  $Re(\lambda) > 0$ , keep increasing  $\kappa_b$  or decreasing  $q_0$  would eventually make  $Re(\lambda)$  negative which means the loss of the ability of amplification. As has been addressed previously, the charge,  $q_0$  depends on the intracellular cations' density ( $K^+$  and  $Ca^{2+}$ ) when the ions channel is open. Thus,  $q_0$  also depends on the cations' density of the environment where the stereocilia located. Higher concentration of cations in the environment leads to larger absolute value of  $q_0$  and vice versa. When the cations' concentration of the environment is too small, the system would become stable and the active motion would disappear. The bending stiffness  $\kappa_b$  of the biomembranes is another key factor that affect the stability of the system. Medicine, for instance, has been known to alter the bending stiffness  $\kappa_b$  of the biomembranes (Fa et al., 2007; Hakizimana and Fridberger, 2015). According to the results shown in Fig. 5, the hair bundle may in such a case, malfunction.

#### 4. Nonlinear analysis of the dynamical behavior of hair bundles

Most prior studies have focused on studying a version of the linearized system in (3.38). To further confirm and investigate the mechanism of the amplification, we carry out a fully numerical study to solve the nonlinear system described by (2.7) and (2.36). The details of the numerical simulation may be found in the Appendix.

To investigate the importance of flexoelectricity to the function of amplification of the hair bundle, we compare the cases with and without the consideration of flexoelectricity. Fig. 6(a) shows the variation of the tip displacement with respect to time without the consideration of flexoelectricity  $f = 0$  as  $\kappa_b = 30k_B T$  and  $q_0 = 0.2mC/m^2$ . Fig. 6(b) shows the result for the case of with flexoelectricity. It is seen from the figure that a slight perturbation is amplified to about 100nm vibration in about 3ms. Comparing Fig. 6(a) and (b) we infer that in the absence of flexoelectricity, the system will lose its ability to amplify small perturbations of sound. This confirms our speculation that the amplification arises flexoelectric effect which converts the energy of ions flow into the deformation of stereocilia.

Regarding the flexoelectric effect, a practical question is how much energy of the flowing ions can be converted into the mechanical energy of stereocilia. In other words, is this energy sufficient to adapt an active motion of hair bundles? To answer this question is not easy. In what follows, we attempt to show how some parameters affect the energy conversion efficiency. From the results we obtained from the linear analysis, it is found that the parameters  $q_0$  and  $\kappa_b$  are critical to the

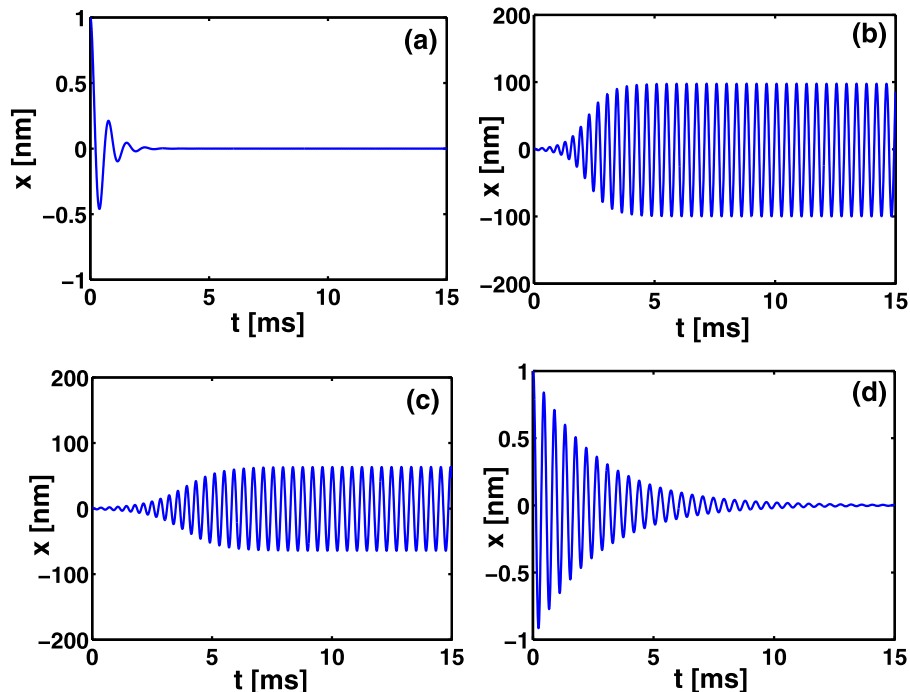


Fig. 6. Tip displacement vs time for  $\kappa_b = 30k_B T$  and (a) without flexoelectricity, (b) with flexoelectricity and  $q_0 = 0.2mC/m^2$ , (c) with flexoelectricity and  $q_0 = 0.15mC/m^2$ , and (d) with flexoelectricity and  $q_0 = 0.08mC/m^2$  under a stimulation of  $F_0 = 1pN$ .

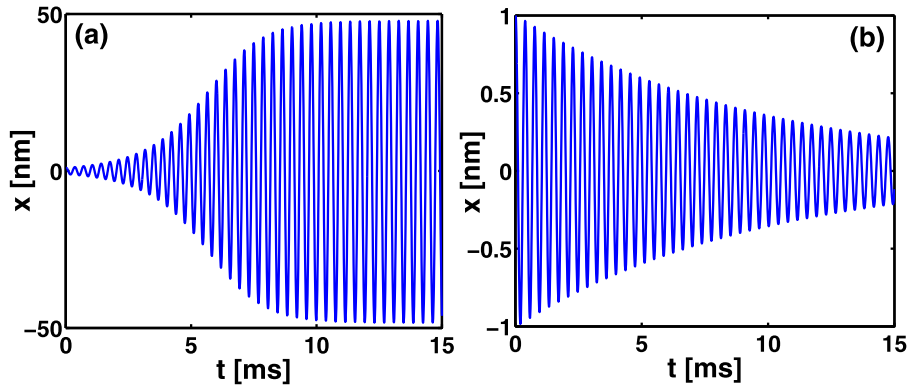


Fig. 7. Tip displacement vs time for  $q_0 = 0.2mC/m^2$  and (a)  $\kappa_b = 40k_B T$ , (b)  $\kappa_b = 50k_B T$  under a stimulation of  $F_0 = 1pN$ .

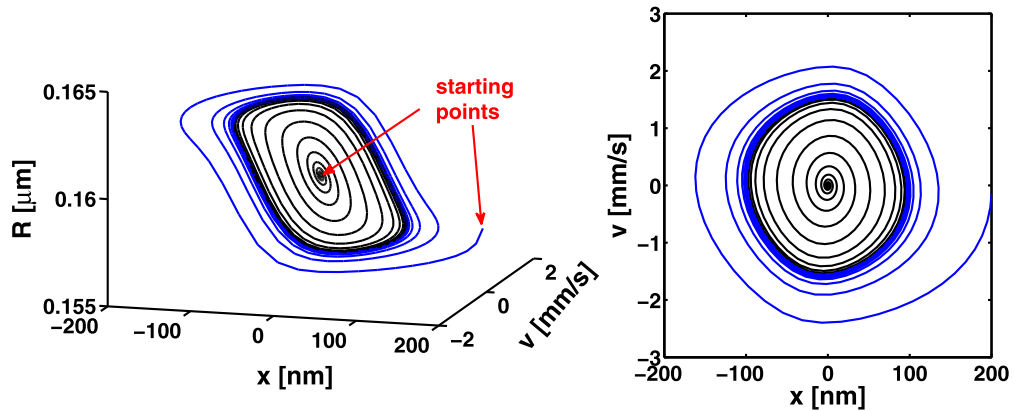


Fig. 8. The 3D (a) and 2D (b) plots of the phase diagram for the vibrating of the stereocilia with  $q_0 = 0.2mC/m^2$  and  $\kappa_b = 30k_B T$ . Starting from different points, the trajectories always converge to the limit cycle.

performance of the dynamic system. So, here we also study the effects of these two parameters on the nonlinear behavior of the system. Fig. 6(c) and (d) give the tip displacement vs time curves for  $\kappa_b$  unchanged but  $q_0$  equals to  $0.15mC/m^2$  and  $0.08mC/m^2$ , respectively. Comparing these two figures with Fig. 6(b), we can easily see that decreasing the absolute value of  $q_0$  suppresses the amplification significantly. As shown in Fig. 6(c), decrease of the absolute value of  $q_0$  by about 25% can reduce the amplitude of the tip displacement by about 50% (around 50nm in magnitude) and increase the time for the amplification to 7ms. When  $q_0$  is further reduced to  $0.08mC/m^2$ , the system loses its function of amplification. This finding indicates that reducing the cations concentration of the environment could lead to the loss of hearing.

In Fig. 7(a) and (b), the effect of bending modulus  $\kappa_b$  on the dynamical behavior of the system is studied. As shown in Fig. 7(a), if we increase  $\kappa_b$  to  $40k_B T$ , the amplitude for the tip displacement decrease to around 50nm and it takes more than 8ms for the vibration of the tip displacement to become stable. If we further increase  $\kappa_b$  into  $50k_B T$ , as shown in Fig. 7(b), the system would lose its ability of amplification. Compare Fig. 7(a) and (b) with Fig. 6(b), we find that increase the membranes' bending modulus  $\kappa_b$  leads to the suppression of the amplification.

Fig. 8 (a) and (b) respectively show the 3D and 2D plot for the phase diagram for the vibration of the stereocilia with  $q_0 = 0.2mC/m^2$  and  $\kappa_b = 30k_B T$ . From the figures, it is found that, starting from different points, the trajectories always converge to a fixed loop which is identified as a limit cycle. An important implication of this is that upon loss of stability, the vibration of the hair bundle will not increase to “infinity” but limits itself. The amplitude of the vibration is always kept to several hundred nanometers. The system therefore exhibits a supercritical Hopf-bifurcation for the chosen parameters. Imagine that a very weak sound wave perturbs the hair bundle by a small distance from its stationary point, the active process will amplify the perturbation towards the radius of the limit cycle. However, for a relatively strong sound wave that perturbs the hair bundle vibrate outside the limit cycle, the active process will attenuate the response and pull the vibration back to the limit cycle. In this way, the hair bundle is protected from extremely strong acoustic stimulations. Although not rigorous, the above mentioned supercritical Hopf-bifurcation is consistent with the reported nonlinear compressibility of the hearing system.

It is interesting to see that the limit cycle shown in Fig. 8(a) and (b) may also partially provide the rationale for the origin of otoacoustic emissions. Mathematically, for a system whose dynamic behavior can be depicted by Fig. 8(a) and (b), an infinitesimally small oscillation about its steady point can be amplified into a detectable oscillation within few ms. Since

flexoelectricity is critical to the existence of the limit cycle, we propose here that otoacoustic emissions are tightly linked with the flexoelectric behavior of the biomembrane.

## 5. Concluding remarks

To understand the sound amplification in the mammalian hearing mechanism, we construct a physical model of the mechanics and dynamics of hair bundles. A key aspect of our work is that we incorporate both membrane electromotility—predicated on the phenomenon of flexoelectricity—as well as a physics-based nonlinear dynamical model. In a departure from prior works, we directly link the mechanical and electrical properties of hair bundles to their performance. We find that, because of flexoelectricity, the oscillation of the hair bundles becomes unstable for some combinations of the inner surface charge density  $q_0$  and the biomembranes' bending stiffness  $\kappa_b$ . The instability endows the system with the ability to amplify very weak acoustic perturbations.

The physical nature of our model allows us to assess in a facile way the effect of external parameters on the performance of the hearing apparatus. For example, we are able to show that the ability of amplification of the stereocilia is due to the Hopf bifurcation related motion of the system. We find that an increase in the bending modulus,  $\kappa_b$  or a decrease in the absolute value of  $q_0$ —both may happen due to illness (Marinkovic et al., 2009; Planells-Cases and Jentsch, 2009) or medicine (Tunstall et al., 1995), may stabilize the system and cause the malfunction of the hair bundle in its function of amplification of external stimulations. In the current model,  $q_0$ , the density of ions that binding to the inner surface of the stereocilia when the ions channel is open, could be linked by future experiments to cations ( $K^+$  and  $Ca^{2+}$ ) concentration of the environment.

## Acknowledgements

The financial support from NSFC (Grant No.11672222), the Fundamental Research Funds for Chinese Central University (XJJ2016071), the M.D. Anderson Professorship of the University of Houston and NIH/NIDCD (R01 DC000354-WEB) are gratefully acknowledged.

## Appendix A

The system of Eqs. (5) and (8) is nonlinear. Analytical solution is not possible. We first rewrite the system of Eqs. (5) and (8) into the following form:

$$\begin{cases} \dot{x}(t) = v \\ \dot{v}(t) = -\frac{c_{eff}}{M_{TM}}v - \frac{K_{eff} - K_L \cos^2 \varphi}{M_{TM}}x - K_L \cos \varphi \sin \varphi \Delta l(R) \\ \quad + F_{stim} \\ \dot{R}(t) = \frac{(\kappa_b - f^2 \epsilon_0 / \eta)}{ch}R + \frac{f q^-(x)}{ch \eta}R^2 + \frac{\Delta t^e}{ch}R^4, \end{cases} \quad (A.1)$$

where the LHS correspond to the time rate of variables  $x$ ,  $v$  and  $R$ . Secondly, forward Euler method is applied for time marching. At time  $t = n\Delta t$  where  $n = 1, 2, 3 \dots$  and  $\Delta t$  being the time step, the time rate of the field variables  $x$  and  $R$  are calculated using (A.1). At last, the values of these two field variables at time  $t + \Delta t$  are estimated by

$$\begin{cases} x(t + \Delta t) = x(t) + \dot{x}(t) \Delta t \\ R(t + \Delta t) = R(t) + \dot{R}(t) \Delta t. \end{cases} \quad (A.2)$$

In the current work, the time step  $\Delta t$  is chosen to be 0.01ms which is small enough for a stable time marching.

## References

- Abdollahi, A., Peco, C., Millán, D., Arroyo, M., Catalan, G., Arias, I., 2015. Fracture toughening and toughness asymmetry induced by flexoelectricity. *Phys. Rev. B* 92 (9), 094101.
- Ahmadpoor, F., Deng, Q., Liu, L., Sharma, P., 2013. Apparent flexoelectricity in lipid bilayer membranes due to external charge and dipolar distributions. *Phys. Rev. E* 88 (5), 050701.
- Ahmadpoor, F., Sharma, P., 2015. Flexoelectricity in two-dimensional crystalline and biological membranes. *Nanoscale* 7, 16555.
- Batters, C., Arthur, C.P., Lin, A., Porter, J., Geeves, M.A., Milligan, R.A., Molloy, J.E., Coluccio, L.M., 2004. Myo1c is designed for the adaption response in the inner ear. *EMBO J.* 23 (7), 1433–1440.
- Breneman, K.D., Brownell, W.E., Rabbitt, R.D., 2009. Hair cell bundles: flexoelectric motors of the inner ear. *PLoS ONE* 4 (4), e5201.
- Brownell, W.E., Qian, F., Anvari, B., 2010. Cell membrane tethers generate mechanical force in response to electrical stimulation. *Biophys. J.* 99 (3), 845–852.
- Brownell, W.E., Spector, A.A., Raphael, R.M., Popel, A.S., 2001. Micro- and nanomechanics of the cochlear outer hair cell. *Annu. Rev. Biomed. Eng.* 3 (1), 169–194.
- Camalet, S., Duke, T., Julicher, F., Prost, J., 2000. Auditory sensitivity provided by self-tuned critical oscillations of hair cells. *Proc. Natl. Acad. Sci. USA* 97 (7), 3183–3188.
- Catalan, G., Lubk, A., Vlooswijk, A.H.G., Snoeck, E., Magen, C., Janssens, A., Rispens, G., Rijnders, G., Blank, D.H.A., Noheda, B., 2010. Flexoelectric rotation of polarization in ferroelectric thin films. *Nat. Mater.* 23 (1), 963.
- Chan, D.K., Hudspeth, A.J., 2005.  $Ca^{2+}$  current-driven nonlinear amplification by the mammalian cochlea *in vitro*. *Nature Neurosci.* 8 (2), 149–155.
- Chandratne, S., Sharma, P., 2012. Coaxing graphene to be piezoelectric. *Appl. Phys. Lett.* 100 (2), 023114.
- Choe, Y., Magnasco, M.O., Hudspeth, A.J., 1998. A model for amplification of hair-bundle of motion by cyclical binding of  $Ca^{2+}$  to mechano-electrical-transduction channels. *Proc. Natl. Acad. Sci. USA* 95, 15321–15326.

- Cooper, N.P., Vavakou, A., van der, H.M., 2018. Vibration hotspots reveal longitudinal funneling of sound-evoked motion in the mammalian cochlea. *Nat. Commun.* 9 (1), 3054.
- Cross, L.E., 2006. Flexoelectric effects: charge separation in insulating solids subjected to elastic strain gradients. *J. Mater. Sci.* 41 (1), 53–63.
- Dalhoff, E., Turcanu, D., Zenner, H.P., Gummer, A.W., 2007. Distortion product otoacoustic emissions measured as vibration on the eardrum of human subjects. *Proc. Natl. Acad. Sci. USA* 104 (5), 1546–1551.
- Deng, Q., Kammoun, M., Erturk, A., Sharma, P., 2014a. Nanoscale flexoelectric energy harvesting. *Int. J. Solids Struct.* 51 (18), 3218–3225.
- Deng, Q., Liu, L., Sharma, P., 2014b. Flexoelectricity in soft materials and biological membranes. *J. Mech. Phys. Solids* 62, 209–227.
- Deng, Q., Liu, L., Sharma, P., 2016. A Continuum Theory of Flexoelectricity. *Flexoelectricity in Solids: From Theory to Applications*. World Scientific.
- Dewey, J.B., Applegate, B.E., Oghalai, J.S., 2019. Amplification and suppression of traveling waves along the mouse organ of corti: evidence for spatial variation in the longitudinal coupling of outer hair cell-generated forces. *J. Neurosci.* 39 (10), 1805–1816.
- Dumitrica, T., Landis, C.M., Yakobson, B.I., 2002. Curvature-induced polarization in carbon nanoshells. *Chem. Phys. Lett.* 360 (1), 182–188.
- Eguiluz, V.M., Ospeck, M., Choe, Y., Hudspeth, A.J., Magnasco, M.O., 2000. Essential nonlinearities in hearing. *Phys. Rev. Lett.* 84 (22), 5232–5235.
- Fa, N., Lins, L., Courtois, P.J., Dufrêne, Y., Smissen, P.V.D., Brasseur, R., Tyteca, D., Mingeot-Leclercq, M.P., 2007. Decrease of elastic moduli of DOPC bilayers induced by a macrolide antibiotic, azithromycin. *Biochimica et Biophysica Acta* 1768, 1830–1838.
- Fettiplace, R., Kim, K.X., 2014. The physiology of mechano-electrical transduction channels in hearing. *Physiol. Rev.* 94, 951–986.
- Gold, T., 1948. Hearing II. the physical basis of the action of the cochlea. *Proc. R. Soc. Lond. B Biol Sci.* 135 (88), 492–498.
- Grati, M., Kachar, B., 2011. Myosin VIIa and sans localization at stereocilia upper tip-link density implicates these usher syndrome proteins in mechanotransduction. *Proc. Natl. Acad. Sci.* 108 (28), 11476–11481.
- Hakizimana, P., Brownell, W.E., Jacob, S., Fridberger, A., 2012. Sound-induced length changes in outer hair cell stereocilia. *Nature Commun.* 3 (1094), 1–7.
- Hakizimana, P., Fridberger, A., 2015. Effects of salicylate on sound-evoked outer hair cell stereocilia deflections. *Pflügers Arch. - Eur. J. Physiol.* 467, 2021–2029.
- Hudspeth, A.J., 1989. How the ear's works work. *Nature* 341, 397–404.
- Hudspeth, A.J., 1997. Mechanical amplification of stimuli by hair cells. *Curr. Opin. Neurobiol.* 7 (4), 480–486.
- Hudspeth, A.J., 2005. How the ear's works work: mechano-electrical transduction and amplification by hair cells. *C.R.Biol.* 328, 155–162.
- Hudspeth, A.J., 2014. Integrating the active process of hair cells with cochlear function. *Nature Rev.* 15, 600–614.
- Hudspeth, A.J., Julicher, F., Martin, P., 2010. A critique of the critical cochlea: Hopf-a bifurcation-is better than none. *J. Neurophysiol.* 104, 1219–1229.
- Kennedy, H.J., Crawford, A.C., Fettiplace, R., 2005. Force generation by mammalian hair bundles supports a role in cochlea amplification. *Nature* 433, 880–883. 2005
- Kern, A., Stoop, R., 2003. Essential Role of couplings between hearing nonlinearities. *Phys. Rev. Lett.* 91 (12), 128101.
- Kothari, M., Cha, M.H., Kim, K.S., 2018. Critical curvature localization in graphene. I. quantum-flexoelectric effect. *Proc. R. Soc. A* 474, 20180054.
- Kothari, M., Cha, M.H., Lefevre, V., Kim, K.S., 2019. Critical curvature localization in graphene. II. non-local flexoelectricity-dielectricity coupling. *Proc. R. Soc. A* 475, 20180671.
- Krichen, S., Sharma, P., 2016. Flexoelectricity: a perspective on an unusual electromechanical coupling. *J. Appl. Mech.* 83, 030801.
- Lakshminarayana, N., 1977. Evaluation of membrane surface charge density: a discussion of some models. *Bull. Math. Biol.* 39, 643–662.
- Liu, L., Sharma, P., 2013. Flexoelectricity and thermal fluctuations of lipid bilayer membranes: renormalization of flexoelectric, dielectric and elastic properties. *Phys. Rev. E* 87 (3), 032715.
- Lumpkin, E.A., Hudspeth, A.J., 1998. Regulation of free Ca<sup>2+</sup> concentration in hair-cell stereocilia. *J. Neurosci.* 18 (16), 6300–6318.
- M. Raphael, R., S. Popel, A., E. Brownell, W., 2000. A membrane bending model of outer hair cell electromotility. *Biophys. J.* 78 (6), 2844–2862.
- Mao, S., Purohit, P., 2015. Defects in flexoelectric solids. *J. Mech. Phys. Solids* 84, 95.
- Maoileidigh, D.O., Hudspeth, A.J., 2013. Effects of cochlear loading on the motility of active outer hair cells. *Proc. Natl. Acad. Sci. USA* 110 (14), 5474–5479.
- Maoileidigh, D., Juicher, F., 2010. The interplay between active hair bundle motility and electromotility in the cochlea. *J. Acoust. Soc. Am.* 128 (3), 1175–1190.
- Maranganti, R., Sharma, N.D., Sharma, P., 2006. Electromechanical coupling in nonpiezoelectric materials due to nanoscale nonlocal size effects: green's function solutions and embedded inclusions. *Rhys. Rev. B* 74 (1), 014110.
- Marinkovic, M., Diez-Silva, M., Pantic, I., Fredberg, J.J., Suresh, S., 2009. Febrile temperature leads to significant stiffening of *Plasmodium falciparum* parasitized erythrocytes. *Am. J. Physiol. Cell Physiol.* 296, C59–C64.
- Martin, P., Hudspeth, A.J., 1999. Active hair-bundle movements can amplify a hair cell's response to oscillatory mechanical stimuli. *Proc. Natl. Acad. Sci. USA* 96 (25), 14306–14311.
- Martin, P., Hudspeth, A.J., 2001. Compressive nonlinearity in the hair bundle's active response to mechanical stimulation. *Proc. Natl. Acad. Sci. USA* 98 (25), 14386–14391.
- Meyer, R.B., 1969. Piezoelectric effects in liquid crystals. *Phys. Rev. Lett.* 22 (18), 918.
- Mosbacher, J., Langer, M., Hörber, J.K.H., Sachs, F., 1998. Voltage-dependent membrane displacements measured by atomic force microscopy. *J. General Physiol.* 111, 65–74.
- Nadrowski, B., Martin, P., Julicher, F., 2004. Active hair-bundle motility harnesses noise to operate near an optimum of mechanosensitivity. *Proc. Natl. Acad. Sci. USA* 101 (33), 12195–12200.
- Nanthakumar, S.S., Zhuang, X., Park, H.S., Rabczuk, T., 2017. Topology optimization of flexoelectric structures. *J. Mech. Phys. Solids* 105, 217–234.
- Nguyen, T.D., Mao, S., Yeh, Y.W., Purohit, P.K., McAlpine, M.C., 2013. Nanoscale flexoelectricity. *Adv. Mater.* 25 (7), 946–974.
- Petrov, A.G., 2001. Flexoelectricity of model and living membranes. *Biochimica et Biophysica Acta* 1561, 1–25.
- Petrov, A.G., 2006. Electricity and mechanics of biomembranes systems: flexoelectricity in living membranes. *Analytica Chimica Acta* 568, 70–83.
- Petrov, A.G., Sokolov, V.S., 1986. Curvature-electric effect in black lipid membranes. *Eur. Biophys. J.* 13 (3), 139–155.
- Planells-Cases, R., Jentsch, T.J., 2009. Chloride channelopathies. *Biochimica et Biophysica Acta* 1792, 173–189.
- Power, R.J., Kulason, S., Atilgan, E., Brownell, W.E., Sun, S.X., Gillespie, P.G., Spector, A.A., 2014. The local forces acting on the mechanotransduction channel in hair cell stereocilia. *Biophys. J.* 106 (11), 2519–2528.
- Power, R.J., Roy, S., Atilgan, E., Brownell, W.E., Sun, S.X., Gillespie, P.G., Spector, A.A., 2012. Stereocilia membrane deformation: implications for the gating spring and mechanotransduction channel. *Biophys. J.* 102 (2), 201–210.
- Rahmati, A.H., Yang, S., Bauer, S., Sharma, P., 2019. Nonlinear bending deformation of soft electrets and prospects for engineering flexoelectricity and transverse ( $d_{31}$ ) piezoelectricity. *Soft Matter* 15, 127–148.
- Rey, A.D., 2008. Linear viscoelastic model for bending and torsional modes in fluid membranes. *Rheol. Acta* 47, 861–871.
- Spiegel, M.F., Waltson, C.S., 1984. Performance on frequency - discrimination tasks by musicians and nonmusicians. *J. Acoust. Soc. Am.* 76, 1690–1695.
- Tinevez, J.Y., Jülicher, F., Martin, P., 2007. Unifying the various incarnations of active hair-bundle motility by the vertebrate hair cell. *Biophys. J.* 93, 4053–4067.
- Tunstall, M.J., Gale, J.E., Ashmore, J.F., 1995. Action of salicylate on membrane capacitance of outer hair cells from the guinea-pig cochlea. *J. Physiol.* 485 (3), 739–752.
- Weitzel, E.K., Tasker, R., Brownell, W.E., 2003. Outer hair cell piezoelectricity: frequency response enhancement and resonance behavior. *J. Acoust. Soc. Am.* 114 (3), 1462–1466.
- Yudin, P.V., Tagantsev, A.K., 2013. Fundamentals of flexoelectricity in solids. *Nanotechnology* 24, 432001.
- Zhang, P., Keleshian, A.M., Sachs, F., 2001. Voltage-induced membrane movement. *Nature* 413, 428–432.
- Zhou, Y., Yang, X., Pan, D., Wang, B., 2018. Improved incorporation of strain gradient elasticity in the flexoelectricity based energy harvesting from nanobeams. *Phys. E* 98, 148–158.
- Zubko, P., Catalan, G., Tagantsev, A.K., 2013. Flexoelectric effect in solids. *Annu. Rev. Mater. Res.* 43 (1), 387–421.